Contrib Mineral Petrol (2000) 138: 35–45

Thilo Arlt · Martin Kunz · Jano Stolz
Thomas Armbruster · Ross J. Angel

P-T-X data on $P2_1/c$-clinopyroxenes and their displacive phase transitions

Received: 19 April 1999 / Accepted: 30 August 1999

Abstract The $P2_1/c$ clinopyroxene kanoite (ideally $MnMgSi_2O_6$) was studied as a function of pressure and temperature using powder X-ray diffraction, differential scanning calorimetry (DSC) and optical methods. The temperature of the $P2_1/c$ to high-temperature (H*T*) $C2/c$ transition ranges from 425 °C in endmember $MnMgSi_2O_6$ to 125 °C in natural samples with an aegirine component. Compiling pigeonite and clinoenstatite–clinoferrosilite literature data, the temperature of the transformation was found to decrease linearly with M2 cation size. A synchrotron powder diffraction study in a heated diamond-anvil cell (DAC) yielded compression and thermal expansion data for low kanoite of composition $Mn_{1.2}Mg_{0.4}Fe_{0.4}Si_2O_6$. The high-pressure (H*P*) phase transition from $P2_1/c$ to H*P* $C2/c$ was reversed at 5.8 GPa at 417 °C. The high-temperature phase transition from $P2_1/c$ to H*T* $C2/c$ was rather indistinct and occurred at approximately 530 °C and 0.76 GPa. In a separate experiment, the H*T* transition was observed optically in a hydrothermal DAC between 0.0 and 0.4 GPa. The *in-situ P-T* data of both experiments yielded an increase in transition temperature with increasing pressure (approx. 149 °C/GPa) and suggest a change in character of the transition from first order to continuous with increasing pressure. The data indicate that the H*T* $C2/c$ and H*P* $C2/c$ polymorphs are distinct phases with different stability fields. Since the high-temperature and the high-pressure polymorphs of kanoite were shown to be isotypic with other low-Ca clinopyroxenes such as the $(Mg,Fe)SiO_3$ series, the conclusions we draw from this study are valid for all clinopyroxenes with small (< 0.88 Å) M1 and M2 cation sizes. The petrologic implications of these conclusions for the occurrence of "clinoenstatite" in the Alpe Arami peridotite are discussed.

T. Arlt · R.J. Angel (✉)
Bayerisches Geoinstitut, Universität Bayreuth,
D-95440 Bayreuth, Germany

M. Kunz
Labor für Kristallographie, ETH Zentrum,
Sonneggstr. 5, CH-8092 Zürich, Switzerland

J. Stolz · T. Armbruster
Laboratorium für chemische und
mineralogische Kristallographie,
Universität Bern, Freiestr. 3,
CH-3012 Bern, Switzerland

Editorial responsibility: V. Trommsdorff

Introduction

Pyroxenes with low-Ca or -Na contents such as enstatite, ferrosilite, pigeonite or kanoite (ideally $MnMgSi_2O_6$), exhibit complicated polymorphism with pressure and temperature. At ambient conditions most of these pyroxenes have primitive space groups, monoclinic $P2_1/c$ or orthorhombic *Pbca*, and structures which are both characterized by two different $[Si_2O_6]$-chain angles. Whereas phase transitions involving orthopyroxenes are reconstructive, clinopyroxenes undergo displacive phase transitions at high temperature (H*T*) as well as at high pressure (H*P*) in which both chains become equal and the symmetry increases to space group $C2/c$. In this paper, the high-temperature form is described as H*T* $C2/c$ while the high-pressure form is denoted H*P* $C2/c$.

The high-temperature transformation of low clinopyroxenes has been investigated extensively by X-ray techniques both in pigeonite $(Mg,Fe,Ca)^{M2}(Mg,Fe)^{M1}Si_2O_6$ (Morimoto and Tokonami 1969; Smyth 1969; Brown et al. 1972; Prewitt et al. 1971) and in the clinoferrosilite–clinoenstatite solid solution $(Fe,Mg)SiO_3$ (Smith 1969; Smyth 1974; Sueno et al. 1984). The phase transitions from $P2_1/c$ to $C2/c$ and *vice versa* are rapid, non-quenchable and reversible; for example the Ca-poor lamellae of exsolved clinopyroxenes (e.g. in volcanic rocks) are found in space group $P2_1/c$ at ambient conditions as a result of inversion from the H*T* $C2/c$ structure. Transition temperatures (to H*T* $C2/c$) range from 1180 °C in clinoenstatite (Shimobayashi and Kitamura 1991) to 200 °C in synthetic pigeonite

$Ca_{0.4}Fe_{1.6}Si_2O_6$ (Prewitt et al. 1971). The latter authors observed that the transition drops with increasing Fe content, but a more general relationship with composition has yet to be developed. Similarly, the pressure dependence of the $P2_1/c$ to HT $C2/c$ phase transition is unknown for any composition.

At upper mantle pressures, the stability of a second $C2/c$ pyroxene polymorph has recently been demonstrated (e.g. Pacalo and Gasparik 1990; Kanzaki 1991; Woodland and Angel 1997). The $P2_1/c$ to HP $C2/c$ phase transition is controlled by the effective cation size, but in addition, the HP $C2/c$ clinopyroxenes may be stabilized by crystal field effects (Arlt et al. 1998). From crystal structure criteria Hugh-Jones et al. (1994) and Arlt et al. (1998) suggested that the HP $C2/c$ and the HT $C2/c$ structures are distinct phases in a thermodynamic sense. Kanoite is of potential interest in this context as the crystal structures of the kanoite polymorphs are isotypic with other low-Ca clinopyroxenes and the high-temperature phase transition is at much lower temperature than for the enstatite–ferrosilite clinopyroxenes (Gordon et al. 1981; Arlt and Armbruster 1997). Kanoite therefore provides an opportunity to study the relationship between the HT and HP $C2/c$ forms. A detailed knowledge of these phases is of particular relevance because relicts of high-pressure clinopyroxene are claimed to have been observed in the Alpe Arami peridotite (Bozhilov et al. 1999) which, if the interpretation is true, would have important consequences for the mechanisms of ultra-high-pressure metamorphism of crustal rocks and their subsequent exhumation. We therefore present the results of a series of experiments on kanoite designed to illuminate the general phase relation of pyroxenes.

Experimental methods

Syntheses

The synthetic kanoite crystals were synthesized using the flux-growth method described by Skogby (1994) and hydrothermal techniques. In the flux run an oxide mixture ($6MnO_2$:$2MgO$:1 Fe_2O_3 mol% in R8059), excess SiO_2 (quartz) and a nutrient to $Na_2B_4O_7$-flux ratio of 2:1 by weight was used. These charges were heated at 1100 °C in a graphite crucible, equilibrated for 24 h, cooled down to 750 °C at 4 °C/h, and finally quenched to room temperature. The crystals were isolated by dissolving the flux with HCl. In the hydrothermal runs R8020, R8024 and R8095, stoichiometric MnO_2-MgO mixtures and an excess of quartz were used. All charges were sealed in Au-capsules and allowed to react 8 days at 750 °C and 0.2 GPa. To increase the crystal size, a small amount of saturated KCl-solution was added to the oxide mix of R8095 (run duration 39 days). The oxygen fugacity was buffered by Ni-rods included as spacers together with the NiO-coating of the bomb walls. The white colour of the run products and a structure refinement on a flux-grown crystal (Arlt et al. 1998) indicate the absence of Mn^{3+}.

Synthesis of clinopyroxenes along the kanoite–diopside join was done in a piston cylinder using (R8007–R8014) glass mixtures as starting materials. The glass was obtained by melting a mixture of $CaCO_3$ + MgO + MnO + SiO_2 at about 1500 °C (2 h) in a graphite crucible under an argon atmosphere and by quenching the melts. The starting mixtures with $(Ca,Mn)MgSi_2O_6$ stoichiometries were loaded dry into small graphite crucibles at 900 °C and 1.5 GPa (internal pressure) with talc as pressure transmitting medium. After a run duration of usually 7–14 days the capsules were quenched to room temperature. The synthesis conditions of all investigated kanoites are summarized in Table 1. The compositions of the run products are given in Tables 2 and 3.

Analytical methods

In addition to synthetic samples, natural kanoite, from Bani Hamid (United Arab Emirates) as already studied by Gnos et al. (1996) and Arlt and Armbruster (1997) were investigated. The chemistry of the grains given in Table 2 represent the compositional spread of kanoite in the same sample (6005). The chemical composition of the natural and synthetic kanoites was determined with a CAMECA SX50 electron microprobe. Synthetic tephroite (Mn), forsterite (Mg), anorthite (Ca), almandine (Fe,Si,Al) and albite (Na) were used as standards. The operating conditions were 15 kV accelerating potential and 20 nA beam current. The acquired signals were corrected for atomic number, mass-absorption and secondary fluorescence effects using the CAMECA-PAP version of the Pouchou and Pichoir (1984) procedure. The clinopyroxene analyses were normalized on the basis of four cations p.f.u. ($M2M1Si_2O_6$) with the Fe^{2+}/Fe^{3+} ratio obtained from charge balance. Due to the small amount of Fe^{3+} in the studied clinopyroxenes, the uncertainty in Fe^{2+}/Fe^{3+} ratios only have a minor effect on our conclusions. Cations were allocated to the M1 and M2 sites according to the procedure described in Morimoto et al. (1988). Site M1 was filled to sum to 1.00 with cations in the order Al^{3+}, Fe^{3+}, Mg^{2+}, Fe^{2+}, Mn^{2+} while M2 was filled to sum to 1.00 with the rest of Mg^{2+}, Fe^{2+}, Mn^{2+} as well as Ca^{2+} and Na^{+}. The effective M1 and M2 cation sizes were then calculated for these occupancies using the cation radii of Shannon (1976).

In natural kanoites and R8059 and R8095, the transition temperature of the $P2_1/c$ to HT $C2/c$ phase transition was measured optically at ambient pressure using a polarizing microscope equipped with a tilting compensator and a LINKAM THMSG 600 heating stage (accuracy ± 1 °C; Arlt and Armbruster 1997). Due to the small crystal size from syntheses R8020 and R8024, differential scanning calorimetry (DSC) and high-temperature Guinier mea-

Table 1 Synthesis conditions of investigated kanoites

Run	Apparatus	Starting material	Capsule	P (GPa)	T (°C)	t (days)	Product
8007	Piston cylinder	Glass mixtures,	Graphite	1.5	900	7	Table 4
8009	Piston cylinder	melted from	Graphite	1.5	900	14	Table 4
8010	Piston cylinder	$CaCO_3$-MnO_2-	Graphite	1.5	900	14	Table 4
8013	Piston cylinder	MgO-SiO_2	Graphite	1.5	900	14	Table 4
8014	Piston cylinder		Graphite	1.5	900	8	Table 4
8020	Hydrothermal	MnO_2-MgO-SiO_2	Au	0.2	750	8	Table 3
8024	Hydrothermal	MnO_2-MgO-SiO_2	Au	0.2	750	8	Table 3
8095	Hydrothermal	MnO_2-MgO-SiO_2	Au	0.2	750	39	Table 3
8059	Flux grown	MnO_2-MgO-Fe_2O_3-SiO_2	Pt-crucible	Atmospheric	1100–750	3.5	Table 3

Table 2 Composition, average cation size and transition temperature of investigated kanoite samples (T_{trans} transition temperature, *Ka* kanoite, *syn* synthetic, *nat* natural)

Clinopyroxene	T_{trans} (°C)	Composition (normalized to $\Sigma = 2$)							Cation size		Source/reference
		Ca	Mn	Fe, total	Fe^{2+}	Fe^{3+}	Mg	Na	Al	M1(Å)	M2(Å)	
Ka,syn	425[a]		0.98				1.02			0.720	0.828	R8020, hydrothermal
Ka,syn	400		1.20		0.40		0.40			0.766	0.830	R8059, flux grown
Ka,syn	400		1.00				1.00			0.720	0.830	R8095, hydrothermal
Ka,syn	385		1.10				0.90			0.731	0.830	R8024, hydrothermal
Ka,nat	330[b]	0.12	1.02				0.86			0.735	0.850	Balmat, USA (Gordon)
Ka,nat	300	0.06	1.02	0.03	0.03	0.00	0.88	0	0	0.714	0.844	Buritirama, Brazil
Ka,nat	260	0.08	0.84	0.01	0.01	0.00	1.04	0.02	0.02	0.723	0.836	Bani Hamid, 6005-79
Ka,nat	250	0.09	0.91	0.03	0.03	0.00	0.91	0.02	0.01	0.698	0.848	Bani Hamid, 6005-26
Ka,nat	240	0.07	0.90	0.04	0.03	0.01	0.95	0.03	0.01	0.718	0.839	Bani Hamid, 6005-17
Ka,nat	230	0.12	0.86	0.03	0.03	0.01	0.96	0.03	0.02	0.732	0.848	Bani Hamid, 6005-83
Ka,nat	195	0.07	0.92	0.07	0.04	0.03	0.90	0.04	0.01	0.730	0.846	Bani Hamid, 6005-23
Ka,nat	165	0.07	0.89	0.10	0.06	0.03	0.85	0.05	0.02	0.704	0.851	Bani Hamid, 6005-88
Ka,nat	160	0.07	0.87	0.10	0.07	0.04	0.85	0.05	0.02	0.688	0.858	Bani Hamid, 6005-90
Ka,nat	150	0.07	0.87	0.11	0.07	0.04	0.85	0.06	0.02	0.702	0.852	Bani Hamid, 6005-34
Ka,nat	150	0.06	0.88	0.11	0.07	0.04	0.83	0.06	0.02	0.693	0.855	Bani Hamid, 6005-91
Ka,nat	125	0.09	0.84	0.14	0.08	0.06	0.80	0.08	0.02	0.696	0.861	Bani Hamid, 6005R-17

[a] Measured with H*T*-Guinier and DSC, all others optically
[b] Value from Gordon et al. (1975; Balmat, New York State)

surements were used to track the phase transition. High-*T* Guinier measurements were performed at the ETH–Zürich on a HUBER diffractometer equipped with a Guinier High-Temperature Chamber 632. The temperature was increased from 350 °C to 840 °C in 35 °C steps. At each step the exposure time was 1.5 hours. Cell parameters were calculated from X-ray powder patterns with the program GIREV. Excess quartz in the experimental products was used as an internal standard. The DSC measurements were done at the Chemistry Department at the University of Bern using a METTLER DSC and GraphWare TA72.

Powder X-ray diffraction experiments (Table 4) were carried out *in situ* at high pressure and temperature in a diamond-anvil cell equipped with a resistance heater (Fei et al. 1992). A 0.2 mm diameter hole in a rhenium gasket, which was pre-indented to a thickness of 0.07 mm, served as the sample chamber. Synthetic kanoite powder (R8059, $Mn_{1.2}Mg_{0.4}Fe_{0.4}Si_2O_6$) was loaded together with NaCl (sample:salt = 2:1), which was used as a pressure indicator. A mixture of methanol and ethanol (4:1) served as the pressure-transmitting medium. A monochromatic [λ = 0.4859(2) Å] X-ray beam was generated by the pair of phased undulators of the ID30 beamline of the ESRF (European Synchrotron Radiation Facility, Grenoble) and selected with a channel-cut Si-(111) monochromator. The powder diffraction patterns were recorded with a fast online image plate reader (Thoms et al. 1998). The 2-d data were first corrected for flatfield effects and inherent detector distortions and then integrated into an intensity versus 2-theta pattern using the program Fit2d according to the procedure described by Hammersley et al. (1996). Final data analysis was done by Rietveld refinement using the program package GSAS (Larson and Von Dreele 1994). Pressure was calculated from the NaCl cell parameter using the equation of state (EoS) given by Birch (1986).

Additional high-*P*-*T* experiments were performed in a hydrothermal diamond-anvil cell at the Bayerisches Geoinstitut. The design of a similar DAC and the method was described in Bassett et al. (1993). A polished section of approx. 60 µm thickness of natural sample 6005 (UAE) was loaded with pure water as hydrostatic pressure medium. The density of the fluid was calculated according to Haar et al. (1984) and the isochore was calculated from the temperature of homogenization of an air bubble in the water using the EoS of Saul and Wagner (1989). The phase transition in kanoite was easily observed under a polarising microscope with crossed polarizers as a spontaneous increase in optical retardation.

EoS of low kanoite and the high-pressure phase transition ($P2_1/c$-HP $C2/c$)

The kanoite powder R8059 with composition $Mn_{1.2}Mg_{0.4}Fe_{0.4}Si_2O_6$ (with the $P2_1/c$ to HT $C2/c$ phase transition observed optically at 400 °C, Table 2) was used in the high-P/high-T synchrotron powder diffraction study. The cell parameters measured at each *P*-*T* point are given in Table 4 and the *P*-*T* path followed is indicated in Fig. 1. With the exception of measurements above 5.9 GPa (hs059–hs062) which were performed in the HP $C2/c$ phase field, and the data points hs083 to hs088 which are considered to be HT $C2/c$, all other *P*-*T* data points lie in the low kanoite ($P2_1/c$) stability field. X-ray reflections of the type h + k = odd (e.g. 2 3 $\bar{3}$) which are forbidden in the $C2/c$ space group but allowed in $P2_1/c$ pyroxenes were observed in low kanoite.

The *P*-*T*-*V* data of low kanoite ($P2_1/c$) given in Table 4 were fit with a 3rd-order Birch-Murnaghan equation of state at high temperature, as proposed by Saxena and Zhang (1990):

Table 3 Composition and cell parameter of cpx along the join kanoite–diopside

Reference/run	X(Ca)[a]	X(Mg)[a]	X(Mn)[a]	a (Å)	b (Å)	c (Å)	β	V (Å^3)	Space group
Ghose et al.	0	1.1	0.9	9.719	8.917	5.248	108.51	431.29	$P2_1/c$
Huebner	0	1.0	1.0	9.732	8.934	5.245	108.52	432.41	$P2_1/c$
Run 8007	0.1	1.0	0.9	9.749	8.932	5.260	108.47	434.38	$P2_1/c$
Run 8010	0.3	1.0	0.7	9.763	8.929	5.278	108.08	437.31	$C2/c$
Run 8009	0.4	1.0	0.6	9.757	8.927	5.276	107.83	437.48	$C2/c$
Run 8014	0.5	1.0	0.5	9.761	8.932	5.270	107.28	438.75	$C2/c$
Run 8013	0.65	1.04	0.31	9.746	8.928	5.262	106.77	438.37	$C2/c$
Bruno et al.	1.0	1.0	0	9.750	8.926	5.251	105.90	439.50	$C2/c$
Sasaki et al.	1.0	1.0	0	9.741	8.919	5.257	105.97	439.10	$C2/c$
Ahn et al.	1.0	1.0	0	9.751	8.931	5.255	105.89	440.15	$C2/c$

[a] Normalized to X(Ca) + X(Mg) + X(Mn) = 2 = M^{2+}; clinopyroxenes $M_2^{2+}Si_2O_6$

$$P = 3/2\,K_{T,0}[(V_{T,0}/V)^{7/3} - (V_{T,0}/V)^{5/3}] \times \{1 - 3/4\,(4 - K'_{T,0})[(V_{T,0}/V)^{2/3} - 1]\}$$

with

$$K_{T,0} = K_{298,0} + (\delta K_{T,0}/\delta T)_p (T - 298)$$

and where $K_{298,0}$ is the bulk modulus at ambient conditions and $(\delta K_{T,0}/\delta T)_p$ is the temperature derivative of the bulk modulus at constant pressure.

The unit-cell volume $V_{T,0}$ is a function of the thermal expansion α:

$$V_{T,0} = V_{298,0} \exp \int_{298}^{T} [\alpha_0 + \alpha_1 T] \mathrm{d}T$$

A preliminary fit of the T versus V data given at ambient pressure by Arlt and Armbruster (1997; 25–200 °C), showed that within the uncertainties of the data no deviation from linearity could be observed. Therefore the quadratic term from thermal expansion, α_1, was set to zero and the zero pressure volume was fixed at $V_{298,0}$ = 437.0 Å. Refining the remaining parameters to the dataset yielded:

$$K_{298,0} = 84(7)\ \mathrm{GPa};\ (\delta K_{T,0}/\delta T)_p = -0.007(12)\ \mathrm{GPa}/K;$$
$$\alpha_0 = 3.9(2) \cdot 10^{-5} K^{-1}, \quad K'_{298,0} = 6(3).$$

The obtained pressure derivative of the bulk modulus $K'_{298,0}$ is close to the value reported for $P2_1/c$ clinoenstatite of 6.6(1.1) GPa (Angel and Hugh-Jones 1994). The calculated bulk modulus of 84(7) GPa for kanoite is lower than those reported for most of the other clinopyroxenes (e.g. $K_{T,0}$ = 104 GPa for diopside; Zhang et al. 1997 or $K_{T,0}$ = 111 GPa for clinoenstatite; Angel and Hugh-Jones 1994). However, it is similar to that of hedenbergite ($K_{T,0}$ = 83 GPa, Zhang and Hafner 1992). In contrast to the compression data, the thermal expansion of low kanoite $\alpha_0 = 3.85(11) \cdot 10^{-5}$ K^{-1} is higher than the thermal expansion determined for $FeSiO_3$ and $MgSiO_3$ pyroxenes ($2.0–3.2 \cdot 10^{-5}$ K^{-1}; Hugh-Jones 1997).

The high-pressure phase transition from $P2_1/c$ to HP $C2/c$ was observed between 5.68 GPa (hs058 at 421.5 °C) and 5.90 GPa (hs062 at 414.8 °C). With the phase transition reversed at 5.79(9) GPa at 417(3) °C and 5.06 GPa at the room-temperature study of Arlt et al. (1998), the slope of the $P2_1/c$ to HP $C2/c$ phase boundary is similar to those reported for ferrosilite (Woodland and Angel 1997).

The high-temperature phase transition ($P2_1/c$-HT $C2/c$)

Compositional dependence

Arlt and Armbruster (1997) showed that the $P2_1/c$-HT $C2/c$ transition is accompanied by non-linear steps in the cell parameters and birefringence. We have now measured similar changes in unit-cell parameters for synthetic kanoite with $Mn_{0.98}Mg_{1.02}Si_2O_6$ composition (R8020) calculated from high-temperature Guinier data between 320 °C and 700 °C (Fig. 2). At 425 °C the $\bar{2}$ 2 1 reflections of both low kanoite ($P2_1/c$) and HT kanoite ($C2/c$) appear at d = 3.020 Å and 3.035 Å. This shows that both polymorphs of kanoite coexist at 425 °C. Although the reason for this coexistence (also observed by Arlt and Armbruster 1997) is not clearly understood yet, metastability or kinetic effects can be excluded. In ZrO_2 a similar behaviour was explained by strain energy stabilization (Subbarao et al. 1974). Differential scanning calorimetry (DSC) on $Mn_{0.98}Mg_{1.02}Si_2O_6$ (R8020) yielded an endothermic peak corresponding to a minimum (the sample included approx. 10 wt% excess quartz) of ΔH (425 °C) = 0.8 kJ/mol. A DSC measurement on the Mn-richer sample $Mn_{1.1}Mg_{0.9}Si_2O_6$ (R8024) gave a lower transition temperature of 385 °C (Table 2). The optical investigation of $MnMgSi_2O_6$ (R8095) showed the coexistence of the $P2_1/c$ and the $C2/c$ phase between 390 °C and 410 °C.

In Table 2, the composition of the investigated natural and synthetic kanoite samples are listed together with the measured transition temperature and calculated effective size of the M2 site. Synthetic kanoites show the $P2_1/c$ to HT $C2/c$ transition between 385 and 425 °C which is significantly higher compared with the transition of natural kanoites (125–330 °C, Table 2). This difference is due to a small Ca content (0.06–0.12 p.f.u.) that occurs in natural kanoites and reduces the transition temperature (e.g. compare samples from Balmat or Buritirama with the synthetic endmember R8095). In

Table 4 *P*, *T* and cell parameters of kanoite measured in a heated diamond anvil cell at ESRF

File	*T* (°C)	*P* (GPa)	a_{NaCl} (Å)	*a* (Å)	*b* (Å)	*c* (Å)	β (°)	*V* (Å^3)	Space group
hs050	25.0 (1)	0.62	5.5946 (3)	9.748 (5)	8.948 (6)	5.256 (3)	108.41 (5)	434.99 (23)	$P2_1/c$
hs051	309.9 (7)	1.53	5.5878 (2)	9.732 (4)	8.940 (5)	5.255 (3)	108.37 (5)	433.91 (22)	$P2_1/c$
hs052	352.9 (5)	1.75	5.5816 (2)	9.728 (5)	8.936 (6)	5.252 (3)	108.29 (5)	433.49 (23)	$P2_1/c$
hs053	400.4 (3)	1.98	5.57531 (17)	9.722 (4)	8.935 (5)	5.250 (2)	108.30 (4)	432.98 (18)	$P2_1/c$
hs054	453.5 (1.5)	2.20	5.57095 (16)	9.717 (4)	8.929 (5)	5.249 (3)	108.35 (5)	432.26 (20)	$P2_1/c$
hs055	497.9 (1)	2.79	5.54198 (11)	9.701 (4)	8.919 (4)	5.240 (2)	108.29 (4)	430.48 (17)	$P2_1/c$
hs056	420.5 (5)	3.69	5.48069 (14)	9.674 (4)	8.877 (5)	5.220 (3)	107.93 (5)	426.50 (21)	$P2_1/c$
hs057	421.2 (7)	4.48	5.44299 (11)	9.647 (3)	8.858 (4)	5.205 (2)	107.77 (4)	423.56 (16)	$P2_1/c$
hs058	421.5 (5)	5.68	5.39180 (14)	9.634 (5)	8.802 (6)	5.196 (3)	107.73 (6)	419.68 (23)	$P2_1/c$
hs059	420.7 (2)	7.44	5.3266 (2)	9.437 (8)	8.794 (7)	5.043 (5)	103.52 (9)	406.92 (35)	H*P* $C2/c$
hs060	415.8 (2)	8.77	5.2829 (2)	9.427 (6)	8.749 (6)	5.025 (3)	103.04 (6)	403.76 (30)	H*P* $C2/c$
hs061	415.1 (1.0)	6.98	5.34206 (17)	9.445 (5)	8.810 (5)	5.038 (3)	103.39 (7)	407.82 (23)	H*P* $C2/c$
hs062	414.8 (3)	5.90	5.38219 (17)	9.461 (6)	8.845 (6)	5.054 (4)	103.57 (7)	411.13 (28)	H*P* $C2/c$
hs063	416.6 (6)	4.51	5.44109 (19)	9.659 (6)	8.850 (7)	5.198 (4)	107.63 (6)	423.47 (27)	$P2_1/c$
hs064	422.0 (3)	3.08	5.51301 (13)	9.682 (3)	8.912 (4)	5.226 (2)	107.96 (4)	428.96 (16)	$P2_1/c$
hs065	426.0 (4)	2.32	5.55859 (13)	9.708 (3)	8.926 (4)	5.246 (2)	108.32 (3)	431.54 (14)	$P2_1/c$
hs066	427.1 (5)	1.87	5.58786 (11)	9.729 (3)	8.952 (3)	5.2512 (16)	108.23 (3)	434.39 (12)	$P2_1/c$
hs067	442.5 (2)	1.85	5.59197 (12)	9.731 (3)	8.957 (3)	5.2509 (17)	108.19 (3)	434.80 (12)	$P2_1/c$
hs068	459.6 (3)	1.85	5.59540 (12)	9.733 (3)	8.959 (3)	5.2521 (17)	108.21 (3)	435.04 (12)	$P2_1/c$
hs069	476.1 (1)	1.84	5.59958 (12)	9.736 (3)	8.963 (3)	5.2532 (17)	108.21 (3)	435.46 (12)	$P2_1/c$
hs070	502.5 (5)	1.83	5.60545 (12)	9.740 (3)	8.966 (3)	5.2554 (18)	108.24 (3)	435.89 (13)	$P2_1/c$
hs071	522.4 (7)	1.82	5.61036 (11)	9.742 (3)	8.968 (3)	5.2580 (18)	108.29 (3)	436.16 (13)	$P2_1/c$
hs072	537.2 (4)	1.81	5.61387 (12)	9.745 (3)	8.969 (3)	5.2599 (18)	108.33 (3)	436.40 (13)	$P2_1/c$
hs073	558.4 (8)	1.88	5.61320 (11)	9.746 (3)	8.971 (3)	5.2602 (18)	108.32 (3)	436.60 (13)	$P2_1/c$
hs074	556.0 (6)	2.04	5.60178 (13)	9.742 (3)	8.967 (3)	5.2568 (18)	108.23 (3)	436.17 (13)	$P2_1/c$
hs075	540.7 (7)	2.03	5.59888 (13)	9.740 (3)	8.966 (3)	5.2560 (16)	108.25 (3)	435.91 (12)	$P2_1/c$
hs076	519.1 (5)	2.00	5.59715 (12)	9.738 (2)	8.965 (3)	5.2554 (16)	108.25 (3)	435.72 (12)	$P2_1/c$
hs077	500.7 (7)	1.95	5.59642 (12)	9.738 (2)	8.964 (3)	5.2554 (16)	108.25 (3)	435.68 (11)	$P2_1/c$
hs078	554.9 (4)	2.04	5.60138 (11)	9.741 (2)	8.968 (3)	5.2566 (16)	108.25 (3)	436.10 (11)	$P2_1/c$
hs079	574.8 (4)	2.06	5.60411 (11)	9.743 (2)	8.970 (3)	5.2579 (16)	108.26 (3)	436.37 (12)	$P2_1/c$
hs080	608.5 (6)	2.00	5.61511 (14)	9.749 (3)	8.973 (4)	5.262 (2)	108.32 (4)	436.98 (16)	$P2_1/c$
hs081	622.0 (4)	1.82	5.63173 (11)	9.757 (3)	8.977 (3)	5.2697 (17)	108.47 (3)	437.79 (13)	$P2_1/c$
hs082	470.5 (5)	0.93	5.66854 (11)	9.767 (4)	8.992 (4)	5.275 (2)	108.60 (3)	439.08 (15)	$P2_1/c$
hs083	571.4 (3)	0.86	5.7004 (2)	9.780 (6)	9.007 (6)	5.285 (3)	108.74 (5)	440.87 (24)	H*T* $C2/c$
hs084	617.1 (1)	0.87	5.71190 (12)	9.796 (3)	9.009 (3)	5.2927 (17)	108.87 (3)	441.99 (13)	H*T* $C2/c$
hs085	604.0 (1.0)	0.86	5.70960 (10)	9.791 (3)	9.010 (3)	5.2899 (16)	108.84 (3)	441.66 (12)	H*T* $C2/c$
hs086	584.0 (6)	0.80	5.70946 (10)	9.792 (3)	9.012 (3)	5.2901 (16)	108.82 (3)	441.87 (12)	H*T* $C2/c$
hs087	565.0 (7)	0.78	5.70700 (11)	9.790 (3)	9.012 (3)	5.2888 (16)	108.80 (3)	441.72 (12)	H*T* $C2/c$
hs088	542 (3)	0.74	5.70372 (12)	9.787 (3)	9.011 (3)	5.2869 (18)	108.77 (3)	441.46 (14)	H*T* $C2/c$
hs089	511.8 (2)	0.78	5.69192 (11)	9.784 (3)	9.003 (3)	5.2844 (15)	108.74 (3)	440.80 (12)	$P2_1/c$
hs090	495.5 (6)	0.78	5.68808 (12)	9.781 (3)	9.002 (3)	5.2835 (16)	108.70 (3)	440.65 (13)	$P2_1/c$
hs091	469.0 (5)	0.83	5.67654 (10)	9.778 (2)	8.997 (2)	5.2826 (12)	108.69 (2)	440.22 (9)	$P2_1/c$
hs092	447.2 (6)	0.85	5.66964 (11)	9.776 (3)	8.996 (3)	5.2818 (14)	108.65 (2)	440.12 (10)	$P2_1/c$
hs093	420.4 (7)	0.85	5.66291 (13)	9.773 (3)	8.992 (3)	5.2795 (16)	108.64 (3)	439.62 (12)	$P2_1/c$
hs095	417.6 (1.3)	0.87	5.66105 (13)	9.775 (4)	8.991 (4)	5.281 (2)	108.66 (3)	439.73 (15)	$P2_1/c$
hs096	414.5 (3)	1.31	5.62509 (17)	9.761 (4)	8.983 (4)	5.270 (2)	108.41 (4)	438.44 (17)	$P2_1/c$
hs097	482.3 (1)	1.44	5.62996 (15)	9.764 (4)	8.983 (4)	5.272 (2)	108.50 (4)	438.51 (16)	$P2_1/c$
hs098	516.3 (1)	1.49	5.63372 (15)	9.766 (4)	8.981 (4)	5.274 (2)	108.54 (3)	438.57 (15)	$P2_1/c$
hs099	556.2 (2)	1.49	5.64291 (12)	9.770 (3)	8.982 (3)	5.2760 (17)	108.59 (3)	438.83 (13)	$P2_1/c$
hs100	594.0 (1)	1.44	5.65565 (10)	9.771 (3)	8.986 (3)	5.2795 (16)	108.63 (3)	439.26 (12)	$P2_1/c$
hs101	611.2 (1)	1.37	5.66529 (11)	9.770 (3)	8.991 (3)	5.2810 (17)	108.64 (3)	439.56 (13)	$P2_1/c$
hs102	631.1 (4)	1.30	5.67625 (11)	9.775 (3)	8.997 (3)	5.2833 (16)	108.67 (3)	440.19 (12)	H*T* C_2/c ?
hs104	633.5 (2)	1.84	5.63223 (13)	9.763 (3)	8.979 (3)	5.2721 (19)	108.51 (3)	438.25 (14)	$P2_1/c$
hs105	635.2 (2)	1.77	5.63824 (12)	9.764 (3)	8.980 (3)	5.2738 (18)	108.54 (3)	438.41 (14)	$P2_1/c$
hs107	635.4 (2)	1.71	5.64345 (11)	9.767 (3)	8.981 (3)	5.2758 (17)	108.59 (3)	438.63 (13)	$P2_1/c$
hs108	636.6 (5)	1.64	5.64917 (11)	9.768 (3)	8.984 (3)	5.2777 (17)	108.60 (3)	438.96 (13)	$P2_1/c$
hs109	635.8 (4)	1.58	5.65371 (9)	9.769 (3)	8.986 (3)	5.2790 (14)	108.62 (2)	439.16 (11)	$P2_1/c$
hs111	639.6 (4)	1.53	5.65859 (9)	9.768 (2)	8.991 (2)	5.2807 (13)	108.63 (2)	439.47 (10)	$P2_1/c$

addition, in natural kanoites from the United Arab Emirates, a strong decrease of transition temperature with increasing Na content (mainly aegirine component) was observed (Fig. 3). The substitution of only 0.01 Na p.f.u. on the M2 site lowers the transition temperature by approximately 25 °C. The observed phase transition in kanoite from Buritirama, Brazil (described by Schultz-Güttler et al. 1986) which is Na-free, perfectly fits this trend (Fig. 3).

Clinopyroxenes along the pseudo-binary join kanoite–diopside show a complete solid solution at temperatures above 700 °C (Gordon et al. 1981) which

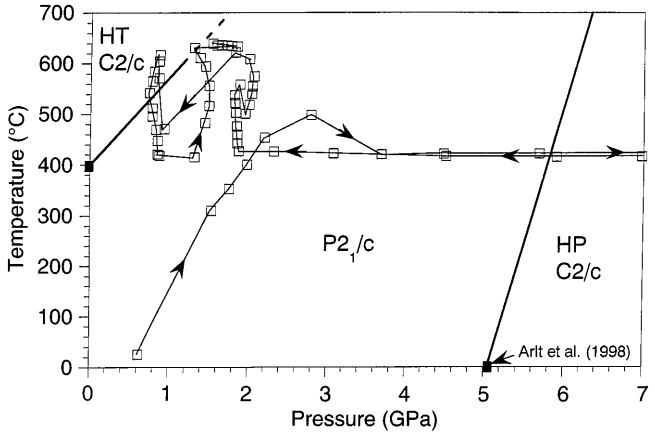

Fig. 1 *P-T* data points measured on kanoite powder in a heated diamond-anvil cell (ESRF). The H*T* phase boundary is from our separate optical study (400 °C at ambient pressure, Table 1; slope 149 °C/GPa, Fig. 6). The H*P* phase transition at ambient temperature is from Arlt et al. (1998)

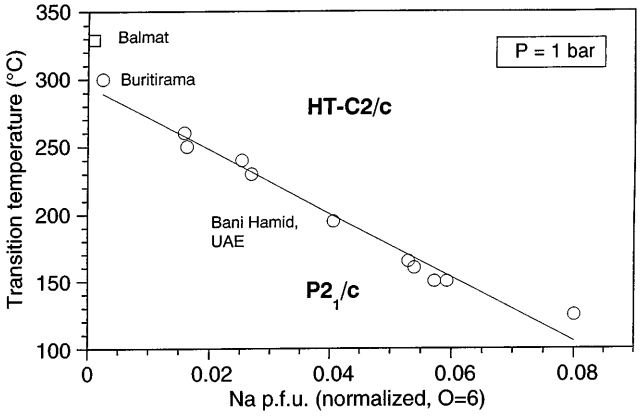

Fig. 3 Transition temperature of the $P2_1/c$ to H*T* $C2/c$ phase transition in natural kanoite as a function of Na content (normalized to 6 oxygen atoms p.f.u.). The *size of symbols* represents the uncertainty of Na measurement (±3%)

Fig. 2 Cell parameters of endmember kanoite $MnMgSi_2O_6$ between 350 °C and 700 °C. The $P2_1/c$-H*T* $C2/c$ phase transition was detected at approximately 425 °C. Errors are represented by the *size of the squares*. ΔV is the volume change involved with the phase transition

was confirmed by the products obtained from our piston-cylinder runs. Due to quenching after the synthesis, exsolution between kanoite and diopside is inhibited. Room-temperature cell parameters calculated from powder X-ray diffraction are given in Table 4 and plotted as a function of composition in Fig. 4 together

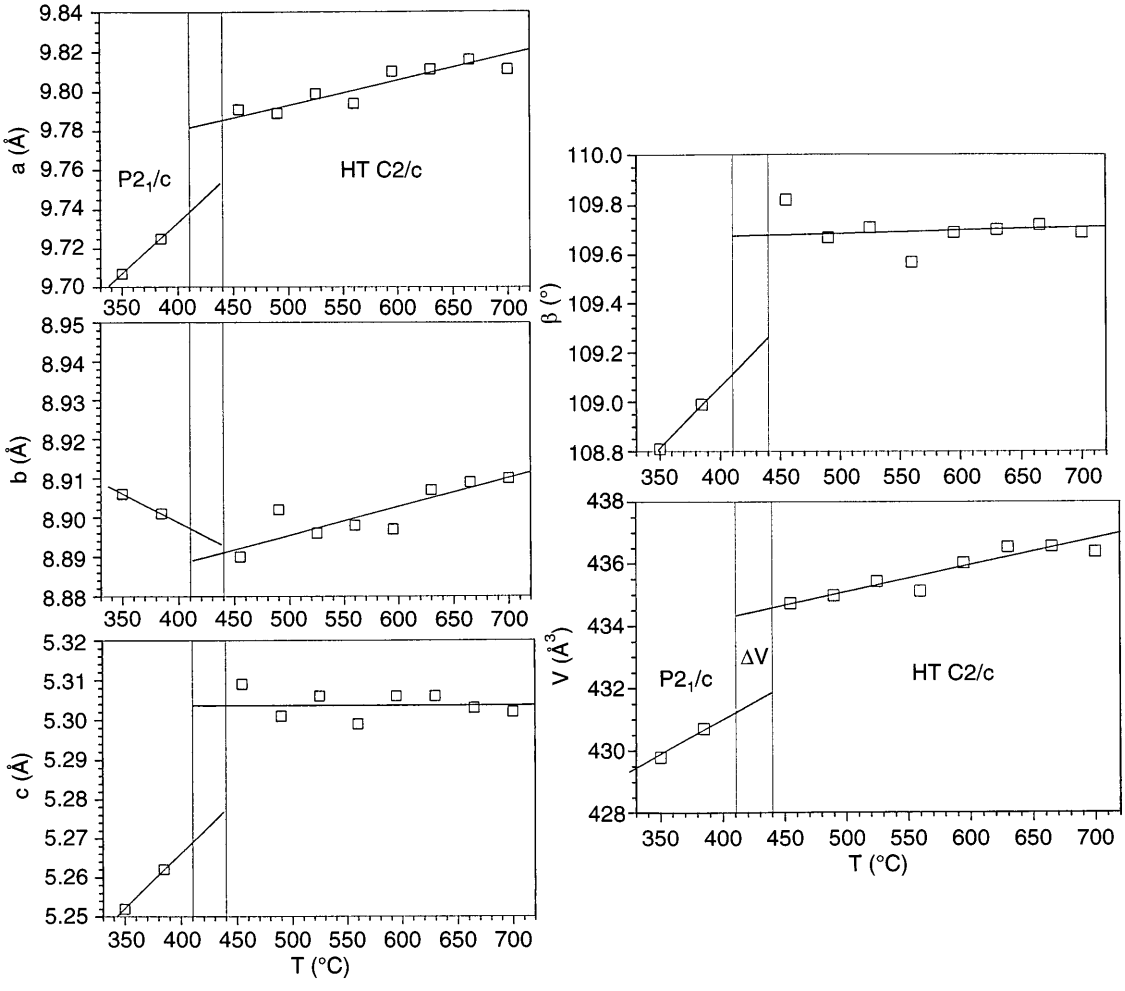

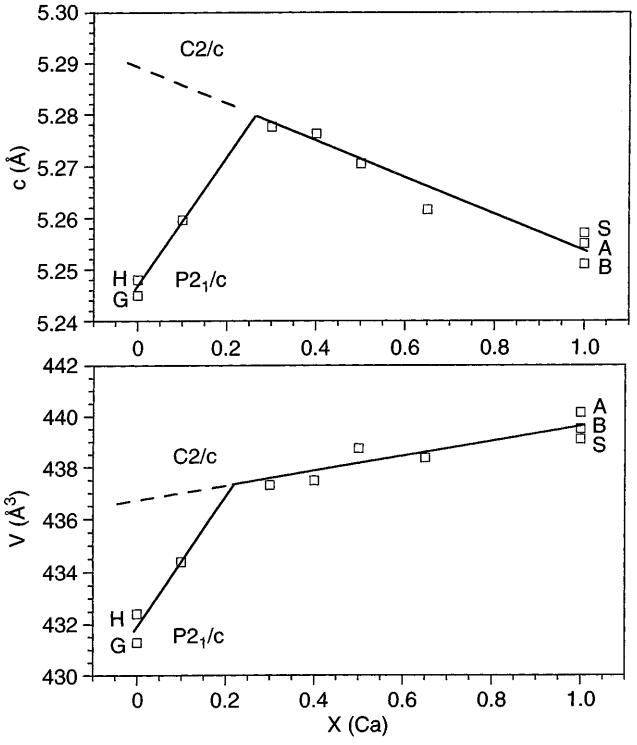

Fig. 4 Cell parameters of clinopyroxene phases along the join $MnMgSi_2O_6$ (kanoite)–$CaMgSi_2O_6$ (diopside). Errors are represented by the *size of the squares*. Kanoite cell parameters were taken from: (*G* Ghose et al. 1975, *H* Huebner 1986) and diopside data are taken from: (*S* Sasaki et al. 1980, *B* Bruno et al. 1982, *A* Ahn et al. 1986)

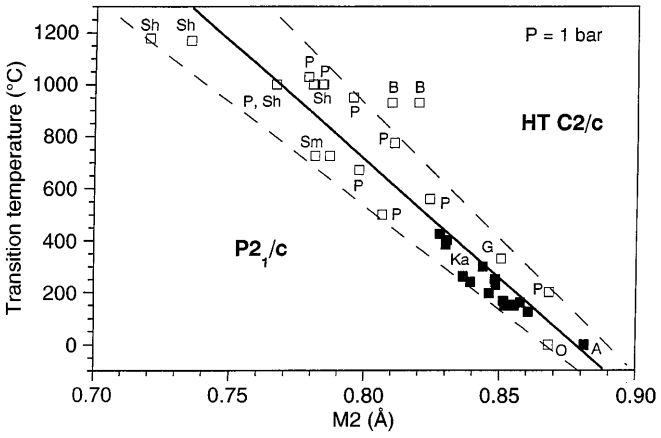

Fig. 5 Compiled data of reported transition temperatures in $P2_1/c$ clinopyroxenes as a function of the average cation size on the M2-octahedral site. (*Solid squares* this study, *open squares* literature data; *Ka* Kanoite data, Table 2, *A* $Ca_{0.3}Mn_{0.7}MgSi_2O_6$, Fig. 2, *B* Brown et al. 1972, *G* Gordon et al. 1981, *O* Ohashi et al. 1975, *P* Prewitt et al. 1971, *Sh* Shimobayashi and Kitamura 1991, *Sm* Smith 1974, *Su* Sueno et al. (1984)

with literature data. The cell dimensions *a* and *c* show a maximum at $X(Ca) \sim 0.3$ ($Mn_{0.7}Ca_{0.3}MgSi_2O_6$), while *b* remains nearly constant (*c* is shown in Fig. 4 top). This non-linearity is also reflected in the monoclinic angle β and in the volume versus X(Ca) plot. The cell volume increases strongly from 432 Å^3 in endmember kanoite to 437 Å^3 at $X(Ca) = 0.3$, whereas there is little volume increase towards the diopside endmember ($V = 439$ Å^3; Fig. 4 bottom). Kanoite-rich clinopyroxenes with $X(Ca) \leq 0.3$ show weak reflections with h+k = odd indicative of space group symmetry $P2_1/c$. The appearance of these reflections indicates that the Ca-poor clinopyroxenes underwent a displacive and non-quenchable phase transition from H*T* *C*2/*c* to $P2_1/c$ during cooling, whereas $(Ca,Mn)MgSi_2O_6$ clinopyroxenes with $X(Ca) \geq 0.3$ possess the space group *C*2/*c* at room temperature. Extrapolation of the diopside data (Fig. 4) yields the cell parameters of a fictive H*T* kanoite endmember with (H*T*) *C*2/*c* space group at room temperature. The convergence of the $P2_1/c$ volumes to those of the *C*2/*c* phase with increasing Ca content indicates that the excess volume due to the *C*2/*c* to $P2_1/c$ phase transition decreases. This behaviour may arise in two different ways. If the transition is first order in character (as in natural kanoites, Arlt and Armbruster 1997) then the data would indicate that the ΔV at the transition decreases with increasing Ca content, becoming zero, coincidentally, at $X(Ca) = 0.30$ ($Ca_{0.3}Mn_{0.7}MgSi_2O_6$) at which composition the transition temperature is 295 K. Such an interpretation would be consistent with our failure to detect the transition by DSC in kanoites with $0.05 \leq X(Ca) \leq 0.15$. Alternatively, if the transition is continuous, then the decrease in the excess volume of the $P2_1/c$ phase with increasing X(Ca) would merely reflect the decreasing transition temperature.

Figure 5 compares the transition temperatures of the $P2_1/c$ to H*T* *C*2/*c* transition of kanoite with literature data (Table 5) on pigeonites, clinoenstatites and clinoferrosilites (Prewitt et al. 1971; Brown et al. 1972; Smyth 1974; Ohashi et al. 1975; Gordon et al. 1981; Sueno et al. 1984; Shimobayashi and Kitamura 1991). The temperature of the $P2_1/c$ to H*T* *C*2/*c* phase transition appears to be a linear function of the average cation size on the M2 site. The data scatter at high temperature is attributable to several other factors including the sensitivity of the apparatus, hysteresis effects, cation disorder, and homogenization of pigeonite-augite lamellae (Prewitt et al. 1971). In contrast to this, problems with cation redistribution and chemical homogenization in kanoite may be ruled out at temperatures below 400 °C. And crystal field stabilization of Fe^{2+}, which was shown strongly to affect the high-pressure phase transition (Arlt et al. 1998; Ross and Sowerby 1999) seems to have a negligible influence on the high-temperature transformation. Since the investigated phase transition is non-quenchable, the trend depicted in Fig. 5 suggests that clinopyroxenes with divalent cations and an average M2 cation size smaller than 0.88 Å occur in space group $P2_1/c$ while those with M2 larger than 0.88 Å at ambient temperature are *C*2/*c* clinopyroxenes. This value is in agreement with the maximum of *a* and *c* at $Ca_{0.3}Mn_{0.7}MgSi_2O_6$ composition (Fig. 4) for which an average (ideal) M2 cation size of $0.3 \cdot 1.00$ Å + $0.7 \cdot 0.83$ Å = 0.88 Å may be calculated. In addition, Ohashi et al. (1975) studied the ferrosilite–

Table 5 Summary of composition, average cation size and transition temperature of (Mg,Fe,Ca)-clinopyroxenes compiled from literature. [*En* clinoenstatite, *Fs* clinoferrosilite, *Pg* pigeonite (Morimoto et al. 1988), T_{trans} temperature of $P2_1/c$ to H*T* $C2/c$ phase transition]. Ionic radii from Shannon (1976)

Clinopyroxene	T_{trans}	Composition ($\Sigma = 2$)			Cation size		
	(°C)	Ca	Fe^{2+}	Mg	M2(Å)	M2(Å)	Reference
En	1180			2.00	0.720	0.720	Shimobayashi
En	1170	0.02	0.16	1.82	0.720	0.735	Shimobayashi
Pg	1000	0.06	0.78	1.16	0.720	0.784	Shimobayashi
Pg	1030	0.08	0.60	1.32	0.720	0.778	Prewitt
Pg	1000	0.10	0.60	1.30	0.720	0.784	Prewitt
Fs	1000		2.00		0.780	0.780	Sueno
En	1000	0.14		1.86	0.720	0.766	Prewitt
Pg	950	0.14	0.60	1.26	0.720	0.795	Prewitt
Pg	930	0.18	1.04	0.78	0.733	0.820	Brown, ideal
Pg	930	0.18	1.04	0.78	0.743	0.810	Brown (960 °C)
Pg	775	0.14	1.16	0.70	0.738	0.811	Prewitt
Fs	725	0.03	1.34	0.62	0.743	0.787	Smyth, ideal
Fs	725	0.03	1.34	0.62	0.749	0.781	Smyth (700 °C)
Pg	670	0.08	1.62	0.30	0.762	0.798	Prewitt
Pg	560	0.20	1.34	0.46	0.752	0.824	Prewitt
Pg	500	0.12	1.46	0.42	0.755	0.806	Prewitt
Pg	200	0.40	1.60		0.780	0.868	Prewitt

hedenbergite join at room temperature and reported the space group change from $P2_1/c$ to $C2/c$ at about $Fe_{1.6}Ca_{0.4}Si_2O_6$ composition. Since the ideal M2 size of that composition is $0.4 \cdot 1.00$ Å + $0.6 \cdot 0.78$ Å = 0.87 Å, their data are in good agreement with Fig. 5. The data that deviate most from the trend shown in Fig. 5 are those for pigeonite from Brown et al. (1972). The authors did not directly determine the composition of their sample, but inferred it from cell parameters. Since their pigeonites contained exsolved augite lamellae, we assume that the cell dimensions implied a Ca content for pigeonite that is too high.

Pressure dependence

In Fig. 1 the observed phase boundaries between the low kanoite ($P2_1/c$) and H*P* kanoite (H*P* $C2/c$) as well as the phase boundary between low kanoite and H*T* kanoite (H*T* $C2/c$) are shown. The high-temperature transition was clearly observed at 400 °C at ambient pressure (Table 2), but rather indistinct at approximately 0.76 GPa and 530 °C. The phase transition is indicated by several weak non-linearities, e.g. the shift of the 2 2 $\bar{1}$ and 3 1 1 reflections and a sharp reduction in the intensity of the 2 3 $\bar{3}$ reflection (data from hs084–hs093). In addition, the cell parameters derived from the measurements hs084 to hs093 were extrapolated to a value of 0.74 GPa (lowest pressure data point hs088) and plotted as a function of temperature. The molar volume *V*, *c*, and especially the *b* cell dimension all clearly show discontinuities between 512 °C and 542 °C (data points hs088, 0.74 GPa and hs089, 0.78 GPa).

In order to confirm the low kanoite to H*T* kanoite (H*T* $C2/c$) transition at 400 °C at ambient pressure, a part of a thick section of the natural UAE-sample with four kanoite grains which shows the lowest transition temperature, (Table 2) were loaded in a hydrothermal (heated) DAC. At atmospheric pressure (without water), the phase transitions in the four grains of slightly different compositions (A, B, C, D) were easily observed optically at 158, 165, 177, and 190 °C, respectively. The composition of grain B is given in Table 2 (Bani Hamid, 6005–88). The composition of the other grains (A, C, and D) was not determined but their transition temperatures indicate that those crystals exhibited slightly different Na concentrations (aegirine component). No hysteresis of the phase transition was observed within the uncertainties of detecting the transition temperature (± 1 °C). After filling the hydrothermal DAC with water as pressure medium, three additional pressure points could be measured in all grains up to 0.4 GPa (Table 6, Fig. 6), but the change of birefringence became weaker

Table 6 Natural kanoite grains in a hydrothermal DAC. Homogenisation temperature and density of the fluid. Temperature and pressure of $P2_1/c$-H*T* $C2/c$ transition

T_H	δ_{H_2O} (g/ml)	Grain[a]	T_{trans}	P (GPa)
In air	–	A	158	0.0
		B	165	0.0
		C	177	0.0
		D	190	0.0
120.1	0.943	A	172	0.090
		B	183	0.110
		C	197	0.136
		D	215	0.170
53.4	0.986	A	195	0.244
		B	201	0.256
		C	222	0.299
		D	237	0.330
30.5	0.9955	A	203	0.289
		B	210	0.303
		C	230	0.345
		D	245	0.377

[a] All grains from sample 6005, Bani Hamid, UAE

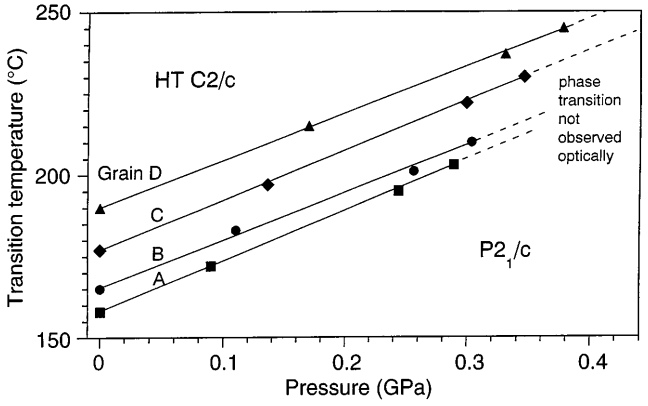

Fig. 6 The $P2_1/c$-HT $C2/c$ phase transition of natural kanoite as a function of P and T, measured in a hydrothermal DAC. The transition was detected by a spontaneous change of retardation on a polarising microscope. *Symbols* represent different grains (*A*, *B*, *C*, *D*) of the same sample with slightly different composition

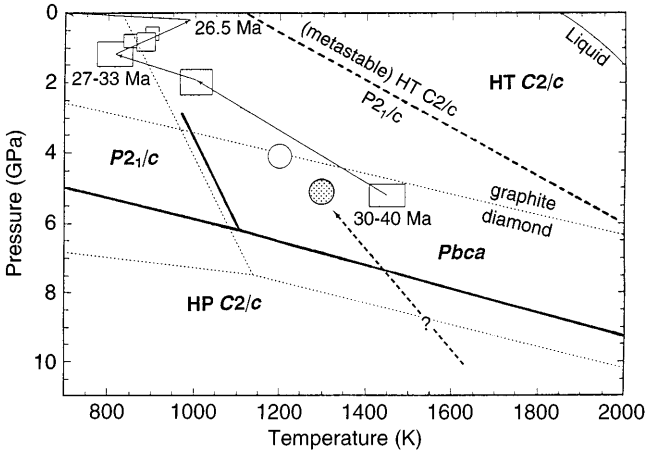

Fig. 7 Exhumation path of the Alpe Arami peridotite modified after Bozhilov et al. (1999). *Open* and *solid circles* and the *boxes connected by solid arrows* represent maximum metamorphic conditions and the exhumation curve determined by previous workers. The phase boundary for $(Mg_{0.9},Fe_{0.1})SiO_3$ (*dotted*) is interpolated from Woodland and Angel (1997). Compared with $(Mg_{0.9},Fe_{0.1})SiO_3$, the *Pbca*-HP $C2/c$ boundary is shifted about 1 GPa towards lower pressure (*solid line*) and the $P2_1/c$-HT $C2/c$ phase boundary estimated for Alpe Arami pigeonite composition is shifted about 700 °C towards lower temperatures (*dashed line*). The *dashed arrow* below 5 GPa is an exhumation path proposed by Bozhilov et al. (1999)

with increasing P/T. Above 0.4 GPa it was not possible to observe the phase transition with optical methods. This indicates that the volume change ΔV_{trans} decreases with pressure and the transition becomes continuous which explains the small changes in the powder diffraction pattern at 0.76 GPa. The suggestion that ΔV goes to zero with increasing pressure is analogous to the apparent decrease in ΔV with increasing Ca-substitution along the diopside–kanoite join (see Fig. 4). The four data points measured on each grain up to 0.4 GPa (Fig. 6), and the weak changes at 0.76 ± 0.02 GPa (approx. 530 °C) suggest a slope of about 149 °C/GPa for the $P2_1/c$ to HT $C2/c$ phase transition and the volume change during the phase transition equals zero above 1 GPa.

Petrologic implications — the Alpe Arami "clinoenstatite"

Recently relicts of high-pressure clinoenstatite were claimed to have been observed in the Alpe Arami peridotite and the conclusion was drawn that these rocks were exhumed from a minimum depth of 250 kilometers (Bozhilov et al. 1999). This interpretation is based on the findings of antiphase boundaries (APBs) which are indicative of the retrograde transformation of either HP $C2/c$ or HT $C2/c$ clinoenstatite to low clinoenstatite ($P2_1/c$). Two arguments led the authors to conclude the high-pressure origin: the orientation of the exsolved clinopyroxene-lamellae and the geological information. Verification of the orientation argument must await further experimental data as already noted by the authors. Their argument against a HT origin was based upon the fact that pure HT clinoenstatite ($MgSiO_3$) only has a small stability field at high T just below the liquidus.

However, Bozhilov et al. (1999) did not consider the strong influence of other cations such as Fe^{2+} and Ca^{2+} etc, on the stability fields of the $C2/c$ forms which is apparent from this study on various clinopyroxenes. The composition of the exsolved clinoenstatite lamellae in Alpe Arami clinopyroxene is $Mg_{1.57}Fe_{0.25}Na_{0.03}Al_{0.02}Ca_{0.14})Si_2O_6$ and therefore it is correctly called pigeonite (Morimoto et al. 1988). In Alpe Arami pigeonite, the effective cation size on the M2 site is 0.783 Å corresponding to a transition temperature of about 850 ± 120 °C (1 bar, Fig. 5) which is about 700 °C lower than the temperature (>1800 °K) assumed by Bozhilov et al. (1999) on the basis of the $MgSiO_3$ phase diagram. Assuming that an average slope of 149 °C/GPa for the $P2_1/c$-HT $C2/c$ phase transition is similar in (Mg,Fe,Ca) clinopyroxenes, the phase boundary for the Alpe Arami composition can be estimated (Fig. 7). Note that this boundary is metastable with respect to orthopyroxene (*Pbca*), but the *Pbca*-HT $C2/c$ boundary will lie at only slightly higher temperatures. The HT $C2/c$ stability field clearly extends to much lower temperatures than assumed by Bozhilov et al. (1999) and could have been accessed without the massif approaching the liquidus. Their argument that the massif would have melted to a large degree or, at minimum, would have left a dominant igneous signature is therefore disproved. Thus inversion of HT $C2/c$ pyroxene at low P remains a possible source of the APBs.

Some confusion exists about the influence of Ca^{2+} on the *Pbca*-HP $C2/c$ phase boundary. Woodland and O'Neill (1995) substituted ferrosilite with Ca^{2+} and found a shift of the phase boundary to higher pressure. The data of Arlt et al. (1998) show that substitution of Mg in enstatite by larger cations reduces the transition pressure of the $P2_1/c$-HP $C2/c$ transformation. The

reduction is about three times larger when crystal field stabilized cations like Fe^{2+} are incorporated. Therefore, substitution of Mg^{2+} by Fe^{2+} or Ca^{2+} strongly increases the stability field of the H*P* *C*2/*c* form due to the larger cation size, whereas substitution of Fe^{2+} by Ca^{2+} decreases it because the total amount of crystal field stabilized ions is reduced. For the given composition of Alpe Arami pigeonite, the $P2_1/c$-H*P* *C*2/*c* transition is estimated to be shifted approximately 2 GPa to lower pressure relative to $MgSiO_3$. According to Woodland and Angel (1997) this shifts the *Pbca*-H*P* *C*2/*c* boundary a minimum of 1 GPa to lower pressures (Fig. 2). Assuming that the Alpe Arami pigeonite indeed formed in the H*P* *C*2/*c* field, a depth of 220 km or higher could have been sufficient. However, if cations remained mobile after the conditions of exsolution then the exsolution may have started at higher Ca contents than that measured in the pigeonite today and thus considerably lower pressures might be assumed.

Figure 7 shows that we are not able to conclude whether Alpe Arami pigeonite was formed in the high-temperature or in the high-pressure *C*2/*c* stability field. In both cases the *C*2/*c* form has to be metastable with respect to transformation to orthopyroxene. Assuming metastability anyway, the possibility of a metastable formation of the *C*2/*c* phase *within* the orthopyroxene stability field must also be considered and appears to be the easiest explanation. However, we have shown that composition has a major effect on the stability fields of both *C*2/*c* phases and as long as there are not sufficient data on pigeonite compositions, it remains highly speculative to suggest a very high pressure origin of Alpe Arami peridotite.

Conclusions

Figure 1 clearly shows that H*T*-kanoite and H*P*-kanoite have separate stability fields which gives further evidence that both phases are indeed distinct, although they exhibit the same space group. This has been suggested earlier from structural considerations (Hugh-Jones et al. 1994; Arlt et al. 1998). In (Mg,Fe)-pyroxenes the $P2_1/c$ phase may gain stabilization by cell doubling at higher temperatures which leads to orthopyroxene (e.g. Woodland and Angel 1997), but the principal relationship between the H*T* *C*2/*c* and the H*P* *C*2/*c* clinopyroxenes is comparable. The stability fields of both *C*2/*c* pyroxenes are separated by pyroxenes with primitive lattices (monoclinic $P2_1/c$ and orthorhombic) in which one of the silicate chains is stretched and the other chain is kinked. Since both chains are stretched in H*T* *C*2/*c* and both chains are kinked in H*P* *C*2/*c*, the $P2_1/c$ clinopyroxenes and orthopyroxenes may be regarded as intermediate structures between high-temperature and high-pressure *C*2/*c* forms. The new data on the phase topology of pyroxenes confirm these structural considerations.

The high-temperature and the high-pressure polymorphs of kanoite were shown to be isotypic with other (Ca,Na)-poor clinopyroxenes such as the $(Mg,Fe)SiO_3$ series and therefore the conclusions we draw from this study are valid for all clinopyroxenes with small (< 0.88 Å) cation sizes. The temperature of the $P2_1/c$ to H*T* *C*2/*c* phase transition is a linear function of the effective M2 cation size. The slope of this phase transition in the *P*-*T* space is approximately 149 °C/GPa and the character of the phase transition changes from first order to a more continuous transition (ΔV goes to zero) as M2 cation size or pressure is increased. The high-temperature and the high-pressure *C*2/*c* polymorphs are distinct phases separated by the stability field of pyroxenes with primitive lattices (monoclinic $P2_1/c$ and orthorhombic). Since both the transition pressure to the H*P* *C*2/*c* phase and the transition temperature to the H*T* *C*2/*c* phase decrease with increasing M2 size, the stability field of "primitive" pyroxenes becomes narrower. As a consequence the stability fields of H*T* *C*2/*c* and H*P* *C*2/*c* phases will meet in the *P*-*T*-*X* space to form one continuous stability field, as is found in the Ca-rich pyroxenes (augite, diopside–hedenbergite).

Acknowledgments The high-temperature studies on kanoite were performed at the University of Bern and financially supported by the Schweizerischer Nationalfonds (Thilo Arlt, Credit 20-33562.92 to T. Peters and Credit 21-26579.89 for the electron microprobe). Edwin Gnos and Tjerk Peters provided the natural kanoite samples. The DSC measurements were performed by R. Giovanoli at the University of Bern. Thomas Wessels helped with the high-temperature Guinier photographs at ETH Zürich. The H*T*-H*P* experiments were done on beamline ID30 of the ESRF. Support from beamline personal is acknowledged. The heatable diamond-anvil cell was lent by François Guyot. Isabelle Daniel and Guillaume Fiquet were very helpful with instructions. At the Bayerisches Geoinstitut, Hans Keppler assisted with the hydrothermal diamond-anvil cell and Helene Bureau helped with the data evaluation. The critical comments of Joe Smyth and two anonymous reviewers improved the quality of the manuscript.

References

Ahn YP, Kim BH, Ishizowa N (1986) Structure refinements of solid solutions in the system CaO*MgO*2SiO_2-Al_2O_3. J Korean Ceram Soc 23: 25–34

Angel RJ, Hugh-Jones DA (1994) Equations of state and thermodynamic properties of enstatite pyroxenes. J Geophys Res 99 (B10): 19777–19783

Arlt T, Armbruster T (1997) The temperature dependent $P2_1/c$-$C2/c$ phase transition in the clinopyroxene kanoite $MnMg[Si_2O_6]$: a single-crystal X-ray and optical study. Eur J Mineral 9: 953–964

Arlt T, Angel RJ, Miletich R, Armbruster T, Peters T (1998) High-pressure $P2_1/c$-$C2/c$ phase transitions in clinopyroxenes: influence of cation size and electronic structure. Am Mineral 83: 1176–1181

Bassett WA, Shen AH, Bucknum M, Ming Chou I (1993) Hydrothermal studies in a new diamond anvil cell up to 10 GPa and from −190 °C to 1200 °C. Pageophysics 141(2/3/4): 487–495

Birch (1986) Equation of state and thermodynamic parameters of NaCl to 300 kbar in the high-temperature domain. J Geophys Res 91(B5): 4949–4954

Brown GE, Prewitt CT, Papike JJ, Sueno S (1972) A comparison of the structures of low and high pigeonite. J Geophys Res 77: 5778–5789

Bruno E, Carbonin S, Molin G (1982) Crystal structures of Ca-rich clinopyroxenes on the $CaMgSi_2O_6$-$Mg_2Si_2O_6$ join. Tschermaks Mineral Petrogr Mitt 29: 223–240

Bozhilov KN, Green HW, Dobrzhinetskaya L (1999) Natural high-pressure clinoenstatite in the Alpe Arami peridotite; additional evidence for a very high pressure origin. Science 284: 128–132

Fei Y, Mao HK, Shu J, Hu J (1992) *P-V-T* equation of state of magnesiowüstite. Phys Chem Miner 18: 416–422

Ghose S, Wan C, Okamura FP (1975) Site preference and transition metal ions in pyroxenes and olivines. Acta Crystallogr Suppl A31, S76, 04: 1–48

Gordon WA, Peacor DR, Brown PE, Essene EJ, Allard LF (1981) Exsolution relationships in a clinopyroxene of average composition $Ca_{0.43}Mn_{0.69}Mg_{0.82}Si_2O_6$ from Balmat, New York: X-ray and scanning transmission electron microscopy. Am Mineral 66: 127–144

Gnos E, Armbruster T, Nyfeler D (1996) Kanoite, donpeacorite and tirodite: Mn-Mg-silicates from a manganiferous quartzite in the United Arab Emirates. Eur J Mineral 8: 251–261

Haar L, Gallagher JS, Kell GS (1984) NBS/NRC steam tables, thermodynamic and transport properties and computer programs for vapor and liquid states of water in SI-units. McGraw Hill, New York

Hammersley AP, Svensson SO, Hanfland M, Fitch AN, Häusermann D (1996) Two-dimensional detector software: from real detector to idealised image or two-theta scan. High Pressure Res 14: 235–248

Huebner JS (1986) Nature of phases synthesized along the join $(Mg,Mn)_2Si_2O_6$. Am Mineral 71: 111–122

Hugh-Jones DA (1997) Thermal expansion of $MgSiO_3$ and $FeSiO_3$ ortho- and clinopyroxenes. Am Mineral 82: 689–696

Hugh-Jones D, Woodland A, Angel R (1994) The structure of high-pressure *C*2/*c* ferrosilite and crystal chemistry of high-pressure *C*2/*c* pyroxenes. Am Mineral 79: 1032–1041

Kanzaki M (1991) Ortho/clinoenstatite transition. Phys Chem Miner 17: 726–730

Larson AC, Von Dreele RB (1994) GSAS, general structure analysis system. Manual, Los Alamos Nat Lab, LAUR 860-748

Morimoto N, Fabriès J, Ferguson AK, Ginzburg IV, et al (1988) Nomenclature of pyroxenes. Am Mineral 73: 1123–1133

Morimoto N, Tokonami M (1969) Domain structure of pigeonite and clinoenstatite up to 700 °C. Neves Jahrb Miner Abh 150: 219–228

Ohashi Y, Burnham CW, Finger LW (1975) The effect of Ca-Fe substitution on the clinopyroxene crystal structure. Am Mineral 60: 423–434

Pacalo REG, Gasparik T (1990) Reversals of the orthoenstatite-clinoenstatite transition at high pressures and high temperatures. J Geophys Res 95: 15853–15858

Pouchou JL, Pichoir F (1984) Un nouveau modèle de calcul pour la microanalyse quantitative par spectrométrie de rayons X. Rech Aerosp 3: 167–192

Prewitt CT, Brown GE, Papike JJ (1971) Apollo 12 clinopyroxenes: high-temperature X-ray diffraction studies. Geochim Cosmochim Acta Suppl 2, 1: 59–68

Ross NL, Sowerby JR (1999) High-pressure crystal field spectra of single crystal clinoferrosillite. Eur J Mineral 11: 791–801

Sasaki S, Fujino K, Takeuchi Y, Sadanaga R (1980) On the estimation of atomic charges by the X-ray method for some oxides and silicates. Acta Crystallogr B36: 904–915

Saul A, Wagner W (1989) A fundamental equation for water covering the range from the melting line to 1273 K at pressures up to 25 000 MPa. J Phys Chem Ref Data 18(4): 1537–1564

Saxena SK, Zhang J (1990) Thermochemical and pressure-volume-temperature systematics of data on solids, example: tungsten and MgO. Phys Chem Miner 17: 45–51

Schultz-Güttler RA, Peters T, Valarelli JV (1986) Constraints on some phase relations in the system CaO-MnO-MgO-K_2O-Al_2O_3-SiO_2-CO_2-H_2O inferred from mineral data from Buritirama, Brazil. Schweiz Mineral Petrol Mitt 66: 281–294

Shannon RD (1976) Revised effective ionic radii and systematic studies of interatomic distances in halides and chalcogenides. Acta Crystallogr A32: 751–767

Shimobayashi N, Kitamura M (1991) Phase transition in Ca-poor clinopyroxenes. Phys Chem Miner 18: 153–160

Skogby H (1994) OH incorporation in synthetic clinopyroxene. Am Mineral 79: 240–249

Smyth JR (1969) Orthopyroxene-high-low-clinopyroxene inversions. Earth Planet Sci Lett 6: 406–407

Smyth JR (1974) The high-temperature crystal chemistry of clinohypersthene. Am Mineral 59: 1069–1082

Smith JV (1969) Magnesium pyroxene at high temperature: Inversion in clinoenstatite. Nature 222: 256–257

Subbarao EC, Maiti HS, Srivastav KK (1974) Martensitic transformation in zirconia. Phys Status Solidi (a) 21: 9–40

Sueno S, Kimata M, Prewitt CW (1984) The crystal structure of high clinoferrosilite. Am Mineral 69: 264–269

Thoms M, Bauchau S, Häusermann D, Kunz M, LeBihan T, Mezouar M, Strawbridge D (1998) An improved X-ray detector for the use at synchrotrons. Nucl Instrum Methods Phys Res A 413: 175–184

Woodland AB, Angel RJ (1997) Reversal of the orthoferrosilite-high-*P* clinoferrosilite transition, a phase diagram for $FeSiO_3$ and implications for the mineralogy of the Earth's upper mantle. Eur J Mineral 9: 245–254

Woodland AB, O'Neill HSC (1995) Phase relations between $Ca_3Fe_2^{3+}Si_3O_{12}Fe_3^{2+}Fe_2^{3+}Si_3O_{12}$ garnet and $CaFeSi_2O_6Fe_2Si_2O_6$ pyroxene solid solutions. Contrib Mineral Petrol 121: 87–98

Zhang L, Hafner SS (1992) High-pressure ^{57}Fe γ resonance and compressibility of $Ca(Fe,Mg)Si_2O_6$ clinopyroxenes. Am Mineral 77: 480–483

Zhang L, Ashbahs H, Hafner SS, Kutoglu A (1997) Single-crystal compression and crystal structure of clinopyroxene up to 10 GPa. Am Mineral 82: 245–258